

Color-switchable nano-silicon fluorescent probes

Huai Chen^{§1}, † Jiang Xu^{§2}, Yaping Wang¹, Da Wang³, Raquel Ferrer-Espada², Yutong Wang⁴,
Jingjian Zhou⁵, Adrián Pedraza-Tardajos³, Mei Yang⁴, Jia-Heng Tan⁶, Xiaoyu Yang⁷, Lei Zhang⁸,
Ilya Sychugov⁵, Shoudeng Chen⁴, Sara Bals³, Johan Paulsson², Zhenyu Yang*¹

1. MOE Laboratory of Bioinorganic and Synthetic Chemistry, Lehn Institute of Functional Materials, School of Chemistry, Sun Yat-sen University, Guangzhou, 510275, China
2. Department of Systems Biology, Blavatnik Institute, Harvard Medical School, Boston, MA, 02115, USA
3. EMAT and NANOLab Center of Excellence, University of Antwerp, B-2020 Antwerp, Belgium, Groenenborgerlaan 171, 2020 Antwerp, Belgium
4. Guangdong Provincial Key Laboratory of Biomedical Imaging, the Fifth Affiliated Hospital, Sun Yat-sen University, Zhuhai, 519000, China
5. Department of Applied Physics, KTH Royal Institute of Technology, 11419 Stockholm, Sweden
6. School of Pharmaceutical Sciences, Sun Yat-sen University, Guangzhou, 510275, China
7. Department of Molecular Medicine, School of Medicine, University of Texas Health Science Center at San Antonio, San Antonio, TX, 78229, USA
8. Department of Chemical Engineering, Waterloo Institute for Nanotechnology, University of Waterloo, 200 University Avenue West, Waterloo, ON N2L3G1, Canada

§ Indicates equal contribution

Corresponding E-mail: yangzhy63@mail.sysu.edu.cn

Abstract

Fluorescent probes are vital to cell imaging by allowing specific parts of cells to be visualized and quantified. Color-switchable probes (CSPs), with tunable emission wavelength upon contact with specific targets, are particularly powerful because they not only eliminate the need to wash away all unbound probe, but also allow for internal controls of probe concentrations, thereby facilitating quantification. Several such CSPs exist and have proven very useful, but not for all key cellular targets. Here we report a pioneering CSP for in-situ cell imaging, using aldehyde-functionalized silicon nanocrystals (SiNCs) that switch their intrinsic photoluminescence (PL) from red to blue quickly when interacting with amino acids in live cells. Though conventional probes often work better in cell-free extracts than in live cells, the SiNCs display the opposite behaviour, and function well and fast in universal cell lines at 37°C, while requiring much higher temperature in extracts. Furthermore, the SiNCs only disperse in cytoplasm not nucleus and their fluorescence intensity correlated linearly with the concentration of fed amino acids. We believe these nano-silicon probes will be promising tools to visualize distribution of amino acids and potentially quantify amino acids-related processes in live cells.

KEYWORDS: silicon, nanocrystal, color-switchable probe, surface chemistry, bio-imaging, photoluminescence

Introduction

Optical imaging is one of the most powerful tools in cell biology, but most assays are only as good as the probes used¹⁻². Probes that are constantly in the on state require excess probe to be washed away to improve the signal-to-noise ratio, which in turn means that the probe must be reintroduced every time labelling is updated (Figure 1a). Activatable probes, that only emit light when interacting with the specific target (Figure 1b), solve that problem, but it is still difficult to assess the total probe concentration in any given location, which in turn makes labelling less quantitative and reliable. Color-switchable probes (CSPs) address that challenge as well, and though they are a relatively new member of the fluorescent probe family, they have proven very powerful by providing more reliable information about cells (Figure 1c). Until now, most CSPs have been based on fluorescent proteins or organic molecular chromophores with various photochemical mechanisms for color-switching, such as Förster resonance energy transfer (FRET) and aggregation-induced emission (AIE)³⁻⁸.

Inorganic semiconductor nanocrystals have emerged as alternatives to conventional probing materials because of their high brightness and stability against degradation and photobleaching⁹⁻¹². However, the photoluminescence (PL) of reported inorganic probes (e.g., semiconductor nanocrystals) have often been insensitive to the cell or tissue environment because the bandgap-based radiative recombination is the dominant emission process. To date, CSPs using inorganic materials with high biocompatibility, suitable for practical bioimaging, have yet to be demonstrated. Silicon nanocrystals (SiNCs) have many advantages over conventional semiconductor nanomaterials because of their highly tunable PL wavelengths, high biocompatibility, and minimal toxicity¹³⁻¹⁹. Unlike other semiconducting nanomaterials, such as II-VI group colloidal quantum dots, the PL of SiNCs can be further tailored by the introduction of

surface ligands²⁰⁻²². Therefore, it exhibits the potential to effectively accumulate the charge carriers generated from the particle core and produce surface-induced PL regardless of the particle size. Theoretically, the SiNCs could effectively switch their intrinsic PL at the red-to-near-infrared region to the surface-trap-based blue PL by incorporating nitrogen moieties on the surfaces (Figure 1d,e). Although there are abundant sources of nitrogen moieties like amino acids (AAs) in the biological environment, such CSP has not been obtained for bioimaging due to its intrinsic sensitivity to cell culture conditions where surface oxidation by oxygen or water can easily quench the PL.

With the aforementioned potentials and limitations in mind, in this work, we report a two-step surface functionalization strategy that can successfully inhibit the oxidation-induced PL loss of SiNCs and investigate its application in cell imaging as a CSP. Hydride-terminated SiNCs (H-SiNCs) with red emission were first passivated by acrolein, and subsequently interacted with various amine species (e.g., AAs, small organic amines and peptides) via a Schiff base reaction mechanism. This two-step passivation approach exhibited an oxidant-inert color-switch from the initial red PL to a surface-induced blue emission, in both cell-free and cytoplasmic environments. In different cell lines with precise control of fed AAs, the in-situ red-to-blue PL switch was found to occur quickly and the blue PL intensity of cells responded in a dose-dependent manner, reflecting distributions and the concentrations of AAs in different intracellular regions. Moreover, this PL switch was only observed within live cells not dead cells, suggesting that some certain biocatalysis in live cells could help overcome high energy barrier of general Schiff base reaction of the SiNCs and AAs in a cell-free environment.

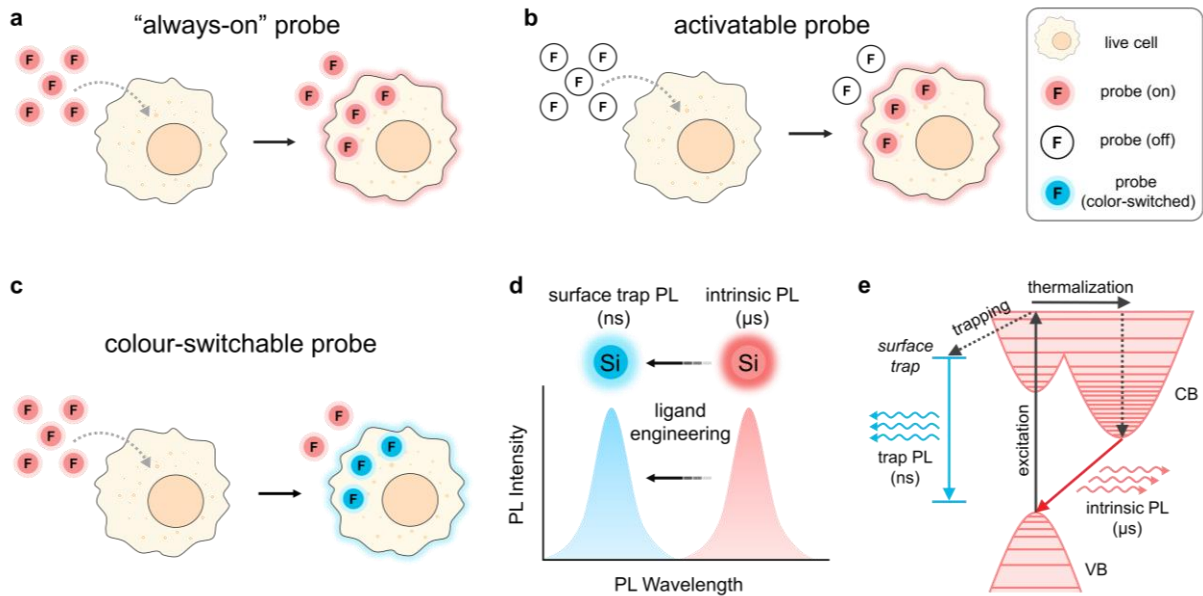


Figure 1. Mechanism of action of existing fluorescent probes and proposed mechanism of action of color-switchable probes. Diagram of the probing mechanism of (a) the “always-on” probe (with continuous fluorescence) and (b) the activatable probe (fluorescence generates only after being bound to the specific target). (c) Proposed color-switchable probe with a fluorescence change after being absorbed and incubated by a cell. (d) Photoluminescence (PL) change of a silicon nanocrystal due to the introduction of the surface states by surface ligand engineering and (e) proposed color-switching mechanism. The intrinsic red PL with slow lifetime decay (μs) is generated from the radiative recombination through the indirect bandgap channel. The introduction of the surface states by ligand engineering in which the exciton recombines radiatively and generates blue PL with fast lifetime decay (ns).

Results and Discussion

Design of a Schiff base Reaction. In the proof-of-concept experiment, the amine sources and SiNCs were bound based on imine structures that were created by Schiff base reactions, a class of condensation method that were commonly used for organic cross-coupling reactions²³. Due to the high yield and functionality at ambient conditions, Schiff base reactions have been widely used in surface chemistry and biotechnology to anchor functional complexes, ligands and biomolecules on substrates²⁴⁻²⁶. Motivated by the benefits of Schiff base reactions and the PL response of H-SiNCs to amine molecules, we devised a surface functionalization approach to anchor organic amines on SiNCs via surface Si-N bonds and Schiff base linkages (Figure 2a). Our goal was to obtain SiNC-based CSPs with PL that can be switched quickly when interacting with biomolecules containing amine groups such as AAs and peptides. We developed a synthetic approach to obtain aldehyde-functionalized SiNCs for further Schiff base reaction.

Specifically, we synthesized a SiNCs/SiO₂ composite via thermal annealing of an amorphous siloxane polymer (HSiO_{1.5})_n obtained from the hydrolysis of trimethoxysilane (see Methods and Figure S1). SiNCs were subsequently liberated by hydrofluoric acid (HF) etching and functionalized by the freshly-prepared ligand acrolein using radical-driven hydrosilylation (Figures 2a, Figures S2-4). This process resulted in red-emitting, aldehyde-functionalized SiNCs (A-SiNCs) of average size ~2 nm as determined using high-angle annular dark-field scanning transmission electron microscopy (HAADF-STEM, Figures 2b, and Figures S5-S7), with a good dispersity in water (Figure S8). FT-IR spectroscopic results (Figure 2c, Figure S9) showed that the original absorption associated with the surface Si-H_x bonds (~2100 cm⁻¹) was replaced by the intense vibration features attributed to C-H_x (~2800-3050 cm⁻¹) and C=O stretching (~1730 cm⁻¹), consistent with surface aldehyde functionalization.

The FT-IR spectrum clearly showed the absence of C=O signal and emergence of C=N stretching signal at $\sim 1700\text{ cm}^{-1}$, indicating the successful formation of the imine linkage (Figure 2c, Figure S10). X-ray photoelectron spectroscopy (XPS) gave insight into the evolution of the elemental oxidation states of SiNCs following surface modification (Figure 2d, e). High-resolution XPS results of A-SiNCs clearly showed the emissions raising only from silicon, carbon, and oxygen. The emission compositions at 99.4 eV, 100.3 eV, 101.5 eV, 102.4 eV, and 103.4 eV can be assigned to elemental silicon, Si-C linkages and silicon suboxides (Figure 2d)²⁷. A new component emerged at 287.4 eV in the carbon 1s spectra of the imine-functionalized SiNCs (Figure 2d), consistent with the formation of imine (C=N) linkage²⁸. An increase of signal intensity of the Si (III) and Si (IV) components occurred in the imine-functionalized SiNCs (Figure 2d), which may be due to the surface Si-N bonds formed from the reaction between the amine end group (-NH₂) and the residual hydride on A-SiNC surfaces²².

We next investigated the effectiveness of Schiff base reaction on A-SiNCs using organic amines (e.g., butylamine (BA), allylamine (ALA), benzylamine (BZA) and phenylethylamine (PEA)). After the reaction for 12 h, a new blue PL appeared and replaced its initial red emission (Figure 2b). TEM analyses confirmed that the red-to-blue PL switch did not come from the change in particle size nor from a change of crystalline nature of SiNCs (Figure 2b; Figure S7). The absorption features of the imine-functionalized SiNCs were similar to that of the original A-SiNCs, as defined by the density of states of the Si core (Figure 2f)²⁹. The initial PL maximum of A-SiNCs was at 880 nm and had a relatively broad PL line width (full width at half maximum, fwhm = 230 nm) (Figure 2g). Following the Schiff base reactions, an emergence of nano-second scale blue PL was observed at 445 - 470 nm, whereas the intrinsic red PL intensity with micro-second scale lifetime was notably diminished (Figure 2g,h). The corresponding PL quantum yield was

decreased (Table S1). We therefore ascribed this to the formation of Si-N surface states that created trap-based radiative recombination pathways, where Si core acted as a sensitizer²².

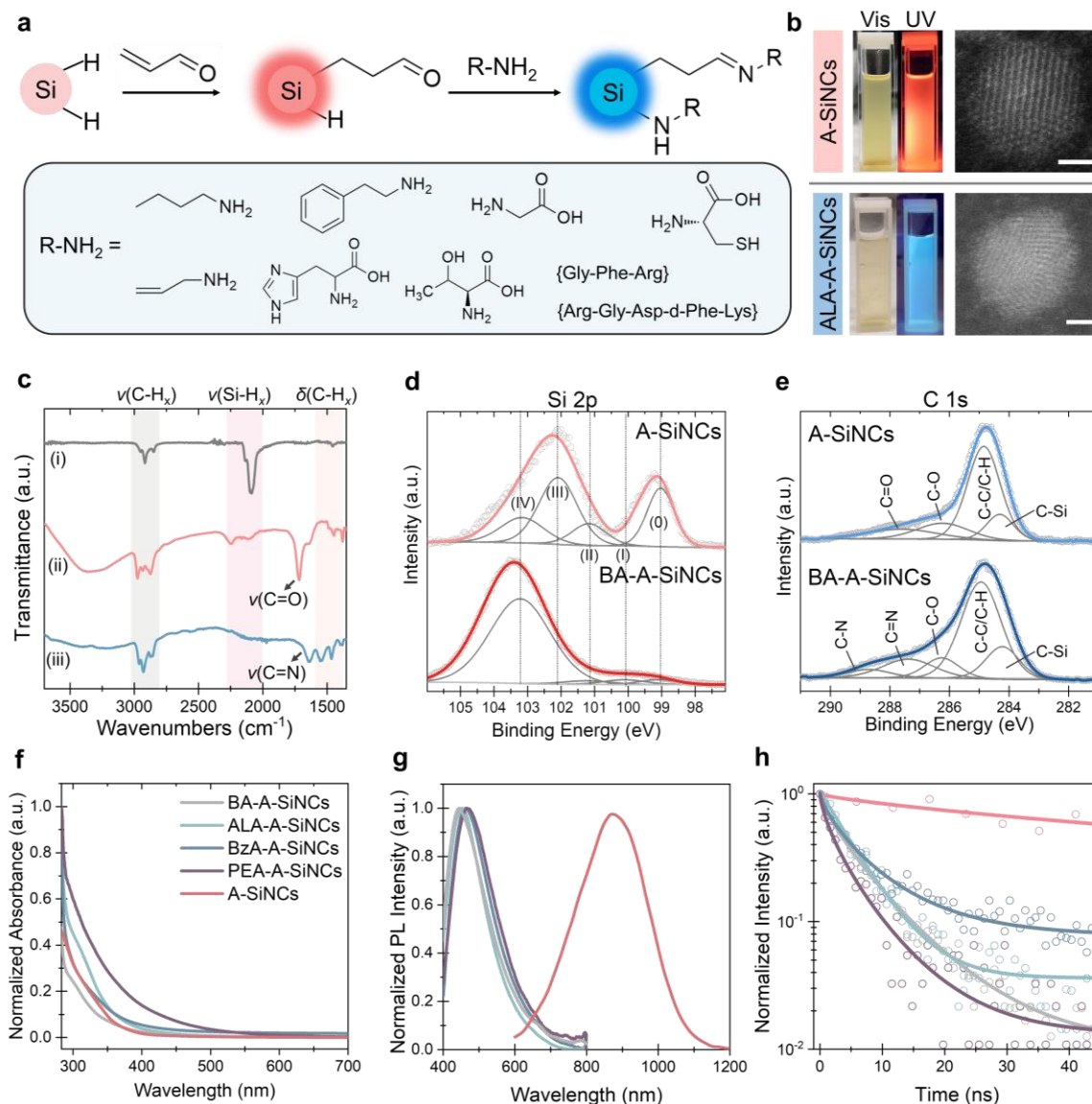


Figure 2. Surface ligand engineering and characterizations of red- and blue-emitting SiNCs.

(a) Schematic representation of the PL change of SiNCs due to a two-step hydrosilylation/Schiff base ligand functionalization. Various types of amines are listed in the box, {Gly-Phe-Arg} and {Arg-Gly-Asp-d-Phe-Lys} represent the peptide sequences. (b) Photograph of aldehyde-passivated SiNCs (A-SiNCs) suspension in chloroform and imine-SiNCs (ALA-A-SiNCs)

suspension in DI water under visible light and UV illumination and HRSTEM images of single SiNCs (scale bar:1 nm). (c) FT-IR spectra of hydride-terminated SiNCs (i), A-SiNCs (ii), and BA-A-SiNCs (iii). High-resolution X-ray photoelectron spectroscopy (XPS) spectra of (d) Si 2p and (e) C 1s regions of A-SiNCs and imine-SiNCs. Fits are shown for the Si 2p_{3/2} emissions. Si 2p_{1/2} components are omitted for clarity. (f) absorption, (g) corresponding PL spectra and (h) PL lifetime decay of A-SiNCs after the reaction with butylamine (BA), allylamine (ALA), benzylamine (BZA), and phenethylamine (PEA).

Schiff base Reactions on Biomolecules. The size-independent PL shift of the imine-functionalized SiNCs suggested that the amine terminal groups can strongly interact with the surface Si-H and C=O bonds. We therefore extended the amine-containing ligands to include AAs, e.g., glycine (Gly), threonine (Thr), L-cysteine (Cys), and L-histidine (His)) and short-chain peptides (e.g., Gly-Phe-Arg (GFR) and Arg-Gly-Asp-d-Phe-Lys (RGD), which widely exist in cells and therefore are ideal as imaging targets. When the AAs and predesigned short-chain peptides were added to the A-SiNC/acetonitrile solution and mixed at 77°C, the intensity of red PL was gradually diminished and a new signal emerges in the blue region (Figure S11). The reaction was complete within 12 h, as indicated by the FT-IR analysis (Figure 3a). No narrowband N-H_x stretching signals (3000 – 3300 cm⁻¹) was observed throughout all the samples in FT-IR studies, suggesting complete removal of unreacted amine sources³⁰⁻³¹. The emergence of C=N features at ~1700 cm⁻¹ and the absence of the sharp C=O stretching signal at 1730 cm⁻¹ from each sample indicated an efficient imine formation on SiNCs. The broad and strong signal at 3000 – 3600 cm⁻¹ was assigned to the O-H stretching mode of the carboxyl groups on the anchored AAs. The spectroscopic features in the 2500 – 3200 cm⁻¹ region can be assigned to the CH_x stretching

and strong intermolecular hydrogen bonding between the carboxylic and ammonium groups on AAs³². We concluded that the Schiff base reaction can also effectively anchor AAs on A-SiNCs through imine linkage and further improve the particle dispersity in water (Figure S8). These chemical bonding features were retained after the reaction in an aqueous environment at 77°C, indicating that the reverse reaction (i.e., hydrolysis of the imine bonds) did not readily occur in the same condition.

We next investigated the influence of AAs and peptides on the optical responses of SiNCs. The absorption in the blue region (below 500 nm) was enhanced after the Schiff base reaction (Figure 3b, Figure 2f and Figure S12). Similar to the observations of the interaction with primary amines (Figure 2), significant PL shifting from red to blue region was observed, and the PL line width was reduced to ~75 nm (Figure 3c, Figure 2g). We then sought to understand the difference in the excitation and emission properties. Static-state excitation-emission-matrix (EEM) spectra (Figure 3d,e) showed that the red-band and blue-band PLs correspond to different excitation regions (red: 360 – 400 nm; blue: 250 – 380 nm). The excitation patterns of A-SiNCs were consistent with those SiNC PLs from the charge carrier recombination at the band-edge whereas the imine-functionalized samples had similar excitation behaviors as previously reported blue-emitting SiNCs due to the radiative recombination at the surface states^{21,33}. Significant changes in photoluminescence quantum yield (PLQY) and PL lifetime decay can be observed after the Schiff base reaction. The photoexcited state lifetime decay value of A-SiNCs was 70 microseconds (Figure 3f and Table S1), similar to previously reported values for alkyl-functionalized SiNCs and can be assigned to the Si core state radiative recombination³⁴. After the interaction with amines, the PL intensity was substantially diminished with a reduced PLQY below 5% (Table S1). The corresponding PL lifetime values were much shorter (i.e., below 10 ns, Fig. 3F and Table S1),

consistent with the fast radiative recombination of carriers in Si surface states introduced due to amine anchoring^{22,33-34}.

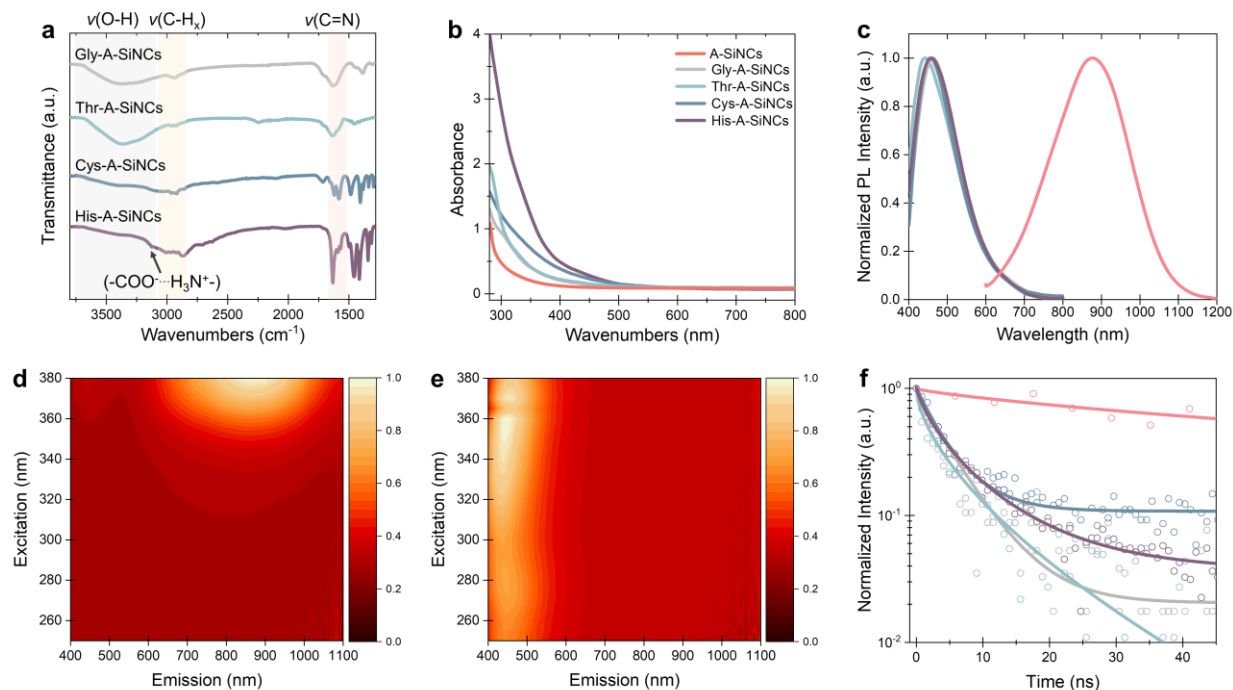


Figure 3. Photophysical properties of amino acid anchored SiNCs. (a) FT-IR, (b) absorption, and (c) photoluminescence spectra of amino acids anchored SiNCs and the original A-SiNCs. Excitation-emission matrix (EEM) PL spectra of (d) A-SiNCs and (e) His-A-SiNCs; (f) PL lifetime decay patterns of A-SiNCs and amino acid anchored SiNCs.

Cells incubation with CSP. Next, to examine the applicability of A-SiNCs as CSPs in live cells, we explored the interaction of A-SiNCs with human acute myeloid leukemia (OCI-AML-2) cells (Figure 4a). The AAs in the culture medium were considered as the main amino supply for cell and thereby we quantitatively set their concentration as a control variable (Supplementary Table 2). In the proof-of-concept experiments, cells were incubated with increasing concentrations of

AAs at 37°C for 24 h, and the phase contrast and fluorescence microscopy images were taken before and after incubation. Initially (i.e., 0 h), we only observed red PL from the A-SiNCs outside the cells under UV excitation. After the 24 h incubation with A-SiNCs, we observed an increase of blue PL inside the cells, indicating that the A-SiNCs had entered the cells and reacted with AAs (Figure 4a,b). Instead of washing away the probe, we can also choose to keep it in the media, to constantly update the labeling, and measure both the red and blue forms for calibration (Figure 4b). In experiments with HeLa cells, we not only observed this red-to-blue PL switch was universal in different cell lines but also found the color switch could take effect in a much shorter time (Figure 4c). Obvious blue fluorescence appeared in the cells after 1 h incubation with a considerable intensity which gradually increased with time (Figure 4d). Since the average division cycle of the HeLa cells was reported to be around 1 day³⁵, the increase of PL intensity of the cells from 1 h to 24 h was most likely correlated to the continuous cell growth and metabolism, with which the uptake of AAs and AA-related reactions were highly involved. More importantly, the intensity of the blue PL increased in a dose-response manner with the AA concentration (Figure 4e) and the concentration of A-SiNCs (Figure S13). The good linear correlation of the AA concentration and the PL intensity indicates the promising potential of SiNC-based CSPs for quantitative bioimaging (Figure 4f).

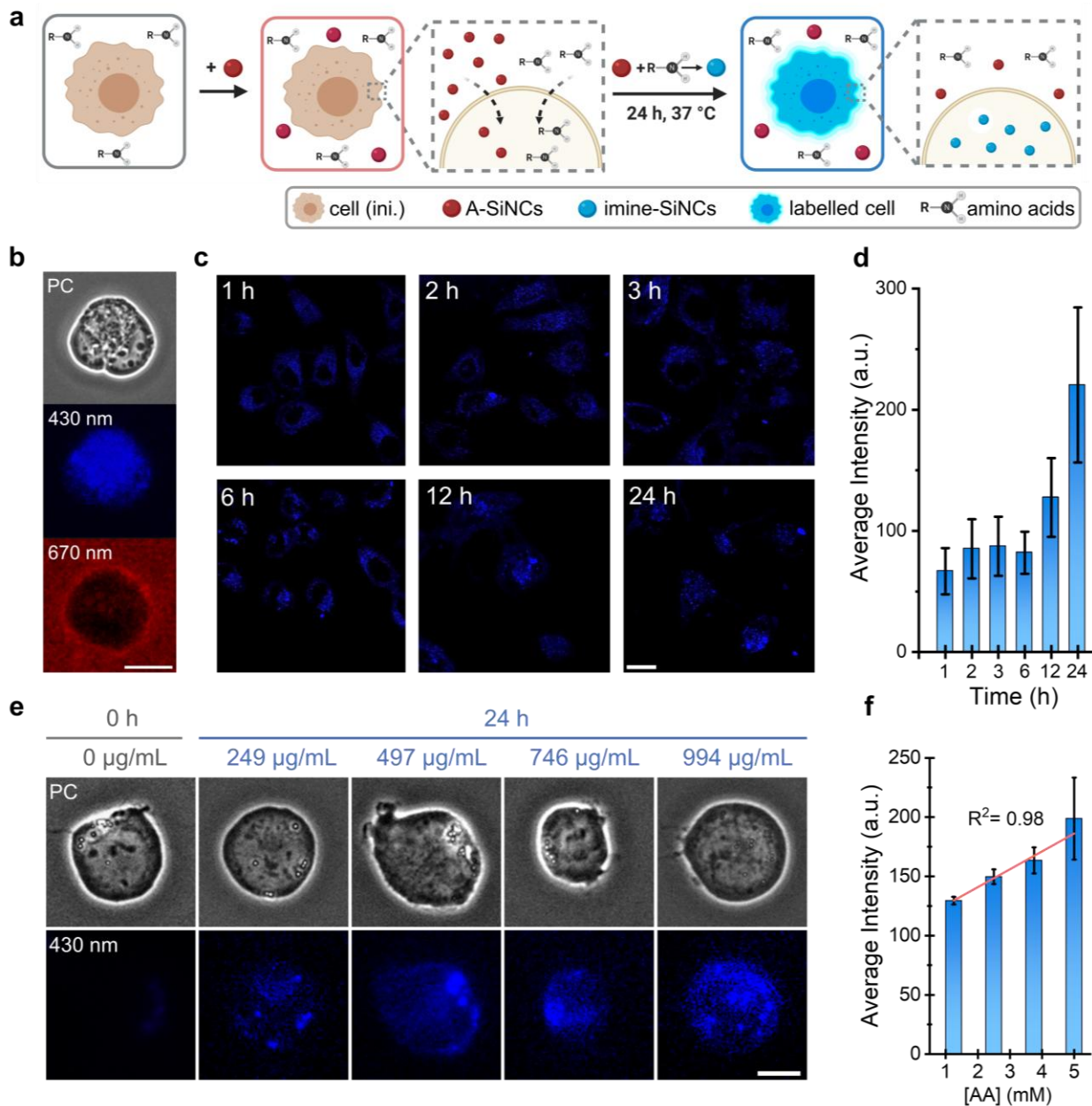


Figure 4. Color-switchable probing of OCI-AML-2 cells and HeLa cells. (a) Schematic diagram of the live cell probing process with A-SiNCs. (b) Representative live OCI-AML-2 cell images after 24h incubation with A-SiNCs. From top to down: Phase contrast (PC), 430 nm (blue), and 670 nm (red) emission wavelengths. $\lambda_{ex\ max} = 408\ nm$ (scale bar: $10\ \mu m$). (c) Representative live HeLa cell images with A-SiNCs after various incubation time (scale bar: $10\ \mu m$). (d) Quantitative

measurements of the emission fluorescence enhancement of cells in Figure 4c. (e) Representative microscopy images of live OCI-AML-2 cells incubated with different AA concentrations. Cells in an AA-free medium (0 $\mu\text{g/mL}$) were taken as a control to compare with cells in different medium containing different amounts of AA (scale bar: 10 μm). (f) Quantitative correlation between the emission fluorescence enhancement of cells and initial AAs feed in Figure 4e. The enhanced intensity equals to the measured intensity minus the intensity of the control group (i.e., 0 $\mu\text{g/mL}$ and 0 h incubation) intensity. Each measurement was repeated three times to obtain an average and standard deviation ($N = 3$). The concentration of A-SiNCs was maintained as 125 $\mu\text{g/mL}$ in Figure 4b, 4c, and 4e, and the concentration of AAs was maintained as 994 $\mu\text{g/mL}$ in Figure 4b and 4c.

AAs tracking by CSP. We were thereby motivated to use the A-SiNCs to probe the intracellular distribution of AAs. For instance, we noticed that during the metaphase and anaphase stages of mitosis (Figure 5a), the intensity of blue fluorescence was much higher in the cytoplasm compared to the nucleus of the cell, suggesting that many more AA-related Schiff base reaction sites are present in the cytoplasm other than the nucleus. We also found that A-SiNCs had significant distribution overlaps with the commercial dyes Lyso-Tracker Green (LTG, labelling lysosome) and Mito-Tracker Green (MTG, labelling mitochondria) (Figure 5b,c), and lysosome and mitochondria are important organelles involved in AA-related cellular reactions³⁶. These findings are not only consistent with previous reports that cytoplasm contains most of AAs in the cell but also confirm the potentials of A-SiNCs for probing AAs in cells^{36,37}.

It is worth noting that the PL-switching behavior of A-SiNCs interacting with AAs occurs at distinctively different conditions. Compared to the relatively slow reaction (12 h) in the cell-free environments at 70°C, similar PL-switching is complete within 1 h at 37°C in cells. We therefore further investigate the role of the intracellular impact on the color-switching of A-SiNCs, we compared the fluorescence signal between living and dead cells (Figure 5d and Figure S14). All cells were stained with the colorimetric dye trypan blue after 24 h of incubation with the A-SiNCs. Trypan blue is a dye commonly used to determine cell viability by exclusively labelling dead cells and its fluorescent effect is negligible under UV excitation. Although impermeable to live cells, it enters and stains dead cells through their compromised cell membrane; this was observed as dark staining in phase-contrast imaging (Figure 5d). We only observed strong blue PL from the live cells, suggesting that the reaction of A-SiNCs and AAs only occurred in live cells. We speculate that the PL-switching undergoes some biocatalytic processes (e.g., enzymatic activity) yet to explore only within the live cells, which significantly reduced the energy barrier of the original Schiff base reactions in cell-free environment³⁸. This comparison showed that this color-switching reaction was closely related to the viability of the cells. Thus, a single probe can separately visualize all cells, and distinguish live and dead ones.

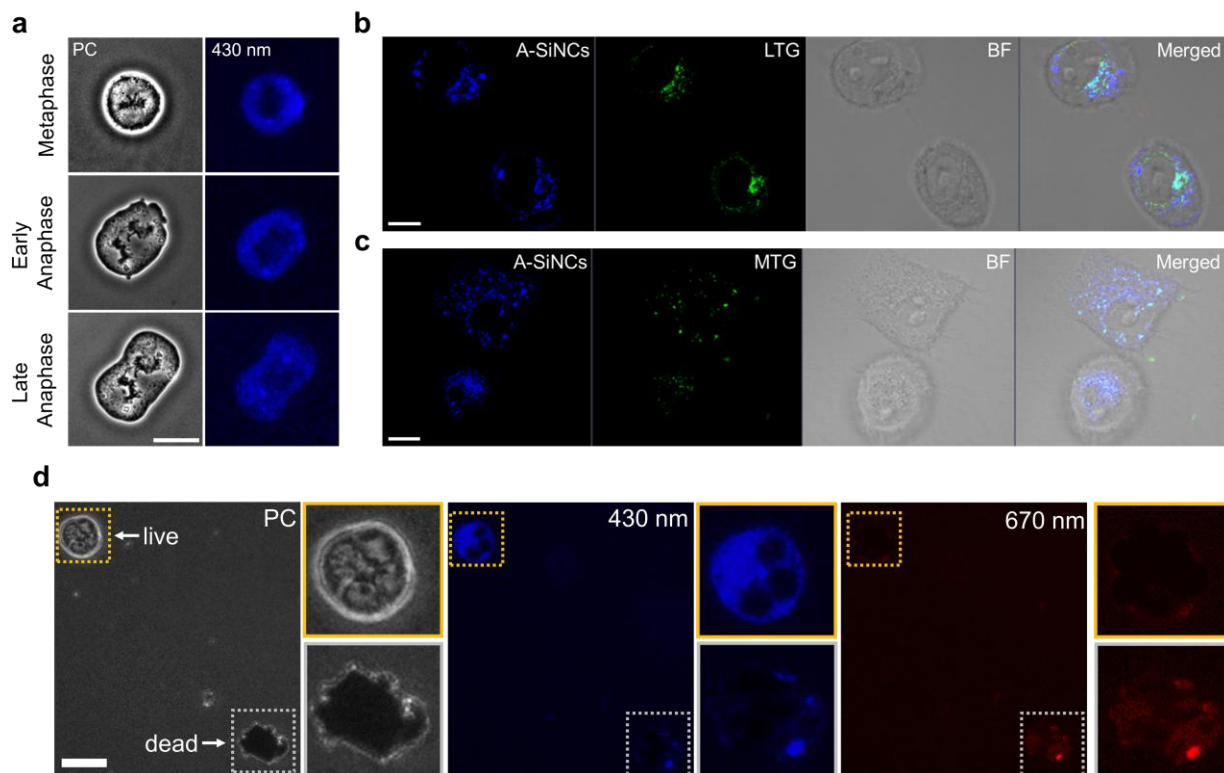


Figure 5. Intracellular response and distribution of A-SiNCs. (a) Probing AAs with A-SiNCs in cells under mitosis. Scale bar: 10 μm . (b) Comparison of the distributions of the A-SiNCs and Lyso-Tracker Green (LTG) in Hela cells. (c) Comparison of distributions of the A-SiNCs and Mito-Tracker Green (MTG) in Hela cells. (d) Live cell responsive manner of A-SiNCs. The live (boxed in yellow) and dead (boxed in grey) OCI-AML-2 cells were classified with a colorimetric dye trypan blue in PC imaging (scale bar: 20 μm). The co-incubation time of the A-SiNCs and cells were 24 h (A-SiNC concentration: 994 $\mu\text{g/mL}$).

4. Conclusion

We herein report a silicon-based color-switchable fluorescent probes with mixed hydride and aldehyde surface groups. Enhanced aqueous dispersity and dramatic color tunability is performed

by this bifunctional surface passivation strategy. The hydride surface groups serve as color-tuned unit to exhibit near-infrared to blue PL transition (> 450 nm) by the strong interactions with amine species. Meanwhile the aldehyde surface groups serve as dispersity-tuned unit to exhibit the hydrophilicity of A-SiNCs at first and homogeneous colloid dispersion by the surface reaction with amine species. These water-soluble SiNC-based CSPs show a clear single-cell resolution and intensity and quantitatively reflect the intracellular concentration and spatial distribution of AAs. They offer a promising path to biosystem probing and to combining with advanced microscopy to develop in-situ cell- or tissue-level, multicolored imaging technology for numerous AA-involved fundamental life activities. This is essential for better understanding of the complex cellular processes as a whole, which cannot be achieved by previous fluorescent probes targeting specific peptides or organelles^{39,40}.

Experimental Section

Materials. All chemicals used are commercially available and were used without any additional purification steps: trimethoxysilane (TMOS, 95%), hydrofluoric acid (HF, 49% aqueous solution, electronic grade), 3,3-diethoxy propene (95%), 2,2'-Azobis-(2,4-dimethylvaleronitrile) (ADVN, 98%), butylamine (BA, 95%), allylamine (ALA, 95%), phenylethylamine (PEA, 95%), glycine (Gly, 99%), L-histidine (His, 99%), L-cysteine (Cys, 99%), and L-threonine (Thr, 99%), ethanol (95%), and chloroform (99.9%) were purchased from Aladdin Chemical Inc. Peptides {H-Gly-Phe-Arg-OH} (G-F-R peptide, powders) and cyclic (Arg-Gly-Asp-D-Phe-Lys) (c(RGDfK), powders) was purchased from GenScript and China Peptides Inc., respectively. For the cell culture experiments, Fetal bovine serum was purchased from ATCC, Penicillin/streptomycin, RPMI

medium with hepes and L-glutamine, Glucose solution, 0.4% trypan blue and distilled water for cell culture media were purchased from thermofisher scientific, RPMI-1640 50x amino acid (AA) solution, sodium bicarbonate, L-Glutamine and hepes were obtained from Sigma-Aldrich and RPMI without L-Glutamine without AA and without Glucose was obtained from My biosource.

Preparation of oxide-embedded silicon nanocrystals (SiNCs). 63 mmol of TriMOS (7.7 mg) was weighed out in a nitrogen-filled glovebox and transferred immediately into a 100-mL Schlenk flask equipped with magnetic stirring under a nitrogen atmosphere. The flask was then soaked in an ice bath to reduce the temperature to $\sim 0^{\circ}\text{C}$. 10 mL of nitric acid (90 mmol) and 10 mL of methanol (25 mmol) were then added into the flask and mixed under a continuous nitrogen flow. Clear and white gels were immediately formed within 5 min. The temperature was then increased to room temperature, and the product was set still without mechanical stirring under a nitrogen atmosphere for 24 h. After the aging process, the product was first isolated from the residual liquid by vacuum filtration and subsequently transferred to a vacuum oven and dried for 16 h. The white, gel-like product was gradually transformed into a blue powder. Approximately 1 g of the powder were then placed in a quartz reaction boat and transferred in a high-temperature tube furnace (Lindberg). The sample was heated from ambient to the predesigned peak temperature of 1100°C at $18^{\circ}\text{C}/\text{min}$ in a slightly reducing atmosphere (5% H_2 + 95% Ar). The sample was maintained at the processing temperature for 1 h and then cooled down to room temperature naturally. The resulting amber-color powdery product was ground manually with a mortar and pestle and then mechanically ground by a ball milling grinder (MSK-SFM-LN-192, MTI KJ Co., Ltd, shaking frequency = 50 Hz, operating time = 3 h). The fine powders were finally stored in a 20-mL vial in ambient conditions for further use.

Liberation of hydride-terminated SiNCs. A conventional HF-etching protocol was applied to liberate SiNCs from the SiO₂ matrix⁴¹. Approximately 0.5 g of the ground product was transferred to a polyethylene terephthalate beaker equipped with a Teflon coated stir bar. 5 mL of ethanol and 5 mL of de-ionized water were added to the beaker with mechanical stirring to form a brown suspension. 5 mL of HF aqueous solution (48% - 51%) was subsequently added into the mixture in ambient conditions under mechanical stirring to initiate the etching reaction (Extreme caution was used when handling the HF solution). After 1 h of etching, the color of the suspension gradually changed to orange. The hydride-terminated SiNCs were extracted from the aqueous solution by multiple additions of toluene (i.e., 3 × 10 mL) and were subsequently transferred to test tubes. The particles were finally isolated from the solution by centrifugation at 4000 rpm for 2 min.

Radical initiated hydrosilylation of acrolein-functionalized SiNCs (A-SiNCs). The ligand acrolein was prepared freshly before the hydrosilylation reaction. 3 mL of 3,3-diethoxy propene was added in a 100-mL polyethylene terephthalate beaker with mechanical stirring. 2 mL of HCl aqueous solution (1 mol/L) was added into the beaker at room temperature to initiate the reaction. After 10 min, the product acrolein was extracted from the water/ethanol solution by the multiple additions of chloroform (i.e., 3 × 5 mL). A trace amount of water was then removed from the product by the addition of 2 g of molecular sieves (3Å) and then used immediately for the hydrosilylation. Hydride-functionalized SiNCs obtained from the centrifugation were redispersed in 15 mL of chloroform (water was removed by the addition of 3Å molecular sieves) and transferred to a dried 100-mL Schlenk flask equipped with a Teflon-coated magnetic stir bar and attached to a nitrogen-charged Schlenk line. Under constant nitrogen flow, 1 mg of the radical initiator 2,2'-Azobis-(2,4-dimethylvaleronitrile) (AVDN, 4 μmol), and the abovementioned,

freshly prepared acrolein was added to the flask under mechanical stirring. The flask was then soaked in an oil bath, and the temperature was increased to 48°C under a static nitrogen atmosphere. The hydrosilylation reaction was maintained for 96 h to yield a transparent orange solution. After the reaction, the functionalized SiNCs were isolated by ultra-centrifugation at 7800 rpm for 20 min. The supernatant was decanted, and the precipitate was redispersed in 20 mL of hexane, followed by another round of centrifugation at 7800 rpm for 20 min. The redispersion/centrifugation/supernatant-removal procedure was repeated twice. Finally, the precipitate was dried in vacuum, stored in a glass vial, and transferred into a nitrogen-filled glovebox for further use.

Schiff base reactions on A-SiNCs. 50 mg of A-SiNCs were weighted out from the glovebox, redispersed in 10 mL of acetonitrile, and transferred to a 35-mL reaction tube equipped with Teflon-coated magnetic stir bar. 0.28 mmol of predesigned organoamines (i.e., butylamine, allylamine, and phenylethylamine) and amino acids (i.e., glycine, L-histidine, L-cysteine, L-threonine) or 0.05 mmol of peptides (i.e., GFR, RGD) were fully dissolved in 20 mL of de-ionized water and then added to the reaction tube and sealed by a Teflon cap. The tube was then soaked in an oil bath, and the temperature was increased to 77°C under a static nitrogen atmosphere. The reaction was maintained for 12 h to yield a transparent light-yellow solution. After the reaction, the solution was cooled down to room temperature. The solvent was completely removed by rotary evaporation, and the powdery imide-functionalized SiNC product was then redispersed in 400 mL of deionized water for dialysis.

Dialysis procedures on SiNCs. The dialysis was carried out with tube dialyzers (15mL, 6-8 kDa, Merck Millipore Inc.). Approximately 10 mL of imide-functionalized SiNC solution was transferred to the tube dialyzer with a foam buoy. The tube dialyzer was then placed in a 500 mL

beaker containing ~400 mL of water and a Teflon-coated magnetic stir bar. Four rounds of dialysis were carried out with a different length of treatment time: first round: 3 h; second round: 8 h; third round: 12 h; fourth round: 15 h. After the dialysis, the purified SiNCs dispersion was extracted and centrifugated; large agglomerates and unfunctionalized particles were removed from the mixed solution using a 0.45 μm PTFE syringe filter.

X-ray diffraction (PXRD) and X-Ray photoelectron spectroscopy (XPS) measurements.

PXRD patterns were collected with a Rigaku Smart Lab diffractometer (Bragg-Brentano geometry, Cu $K\alpha_1$ radiation, $\lambda = 1.54056 \text{ \AA}$). The spectra were scanned between 2θ ranges of $10\text{--}80^\circ$ with an integration of 350 mins. XPS measurements were carried out using the KAlpha XPS system (Thermo Scientific Inc.) with a monochromatic Al $K\alpha$ X-ray source (1486.7 eV, 400 μm spot size). The kinetic energy of the electrons was measured by an energy analyzer operated in the constant analyzer energy mode at 100 eV pass energy for elemental spectra. Casa XPS software (VAMAS) was used to interpret the high-resolution (HR) XP spectra. All spectra were internally calibrated to the C 1s emission (284.8 eV).

Transmission Electron Microscopy measurements. High-resolution high-angle annular dark field-scanning transmission electron microscopy (HAADF-STEM) images were acquired using a cubed Thermo Fischer Scientific electron microscope operated at 300 kV, with a semi-convergence angle of 20 mrad. 10 μL of SiNC solution (2 mg/mL) was drop-casted on a graphene grid and dried in vacuum overnight before use. The analysis of the particle size distribution (PSD) of each type of SiNC was based on multiple images taken from the same sample grid. Over 150 particles were measured for the preparation of the PSD summary of each sample.

Fourier-transform infrared spectroscopy (FT-IR). FT-IR spectra of the SiNCs solid samples were recorded by Nicolet/Nexus-670 FT-IR spectrometer in the region of 4000-400 cm^{-1} equipped with ATR transmission module.

Nuclear magnetic resonance (NMR) analysis. Liquid-state ^1H NMR spectra were recorded using a Bruker Avance III 400 FT-NMR spectrometer by dissolving the desired samples in CDCl_3 .

Absorption and photoluminescence measurements. The UV-Vis spectra of SiNC solutions were measured using a Shimadzu UV-2450 spectrophotometer. Relative absorption spectra were obtained by subtracting and normalizing with/without sample transmission spectra. Photoluminescence (PL) spectra of the SiNCs dispersions were recorded at room temperature using an FLS 980 spectrometer (Edinburgh Instruments) with a Xenon lamp as a continuous wave light source. The excitation wavelength was set as 365 nm for all samples. For spectrally-resolved PL decay measurements, ~ 2 mL of SiNCs/ chloroform solution was transferred in a quartz cuvette. The sample was pumped by a 405 nm laser ($2 \text{ W}/\text{cm}^2$). The spectral resolution of this method is ~ 6 nm. The laser pulse width and repetition rate were set between 100-500 μs and 0.5-10 kHz, respectively. The emitted photons were collected with a 10×0.25 NA objective and sent to a 20×20 μm avalanche photodiode (Becker & Hickl, DPC-230) via spectrometer (Andor Shamrock 500).

Quantum yield measurements. Photoluminescence quantum yield (PLQY) measurements were carried out by home-built integrating sphere setup. Here, a laser-driven xenon plasma white-light source (Energetiq EQ-99) coupled with a tunable monochromator was used as excitation source, a 6-inch diameter integrating sphere (Labsphere) provides light collection, and Peltier element cooled CCD camera (-75°C , Princeton Instruments) is connected to a spectrometer for the signal acquisition. The setup components were connected to an integration sphere with multimode optical

fibers. The system response curve was obtained using an excitation source with a monochromator, where calibration was performed with an optical powermeter. This procedure was executed for spectrometer grating center wavelengths used in measurements. The spectra of SiNC solutions and the corresponding control samples (e.g., toluene, chloroform, de-ionized water) were corrected using a system response curve and subtracted from each other. Unless otherwise specified, the excitation at 380 nm was employed for all the samples. The absolute photoluminescence quantum yield was then calculated by the ratio of absorbed and emitted photons.

Cell culture conditions. OCI-AML-2 cells were cultured in RPMI 1640 media, L-glutamine, and 25 mM of HEPES (Thermo Fisher Scientific) with 10% Fetal Bovine Serum (FBS, ATCC) and 1% Penicillin/Streptomycin solution (Thermo Fisher Scientific) at 37°C and 5% CO₂. The viability and cell number were assessed before experiments with a Bio-rad TC20 automated cell counter and 0.4% trypan blue (Thermo Fisher Scientific).

Preparation of cell culture with different concentrations of A-SiNCs. OCI-AML-2 cells (4 x 10⁴ cell/well) were seeded in RPMI 1640 media containing L-Glutamine, and 25 mM of HEPES (Thermo Fisher Scientific) with 10% FBS (ATCC), 1% Penicillin/Streptomycin solution (Thermo Fisher Scientific) in a 96-well plate and treated with different concentrations of A-SiNCs (0, 31.25, 62.5, 125 and 250 µg/mL) at 37°C and 5% CO₂ for 24 h.

Preparation of cell culture with different concentrations of amino acids. CI-AML-2 cells (4 x 10⁴ cell/well) were incubated with 125 µg/mL of A-SiNCs and different concentrations of AAs for 24 hours at 37°C and 5% CO₂. To prepare the media with different concentration of AAs, 1.85 g of RPMI without L-glutamine, without AA and without glucose was dissolved in 200 ml of dd H₂O, stirring until completely solubilized. 0.5 g of sodium bicarbonate was added with stirring and

the pH was adjusted to 7.4. Glucose, Hepes, FBS, and penicillin/streptomycin were added to a final concentration of 2 g/L, 25 mM, 10% and 1%, respectively. Additional water was added to bring the solution to 250 mL and the media was filter-sterilize using a 0.22 μ m membrane. The 50x AAs solution and L-glutamine were diluted to a final concentration of 1x, 0.75x, 0.5x, 0.25x and 0x (Supplementary Table 2).

Distinguishing live and dead cells. 0.4% trypan blue was used to determine the viability of the cells stained with 125 μ g/mL of A-SiNCs. Briefly, 10 μ L of cell suspension was mixed with 10 μ L of 0.4% trypan blue. The mixture was observed under microscope.

Fluorescence imaging of cells. Stained cells were imaged in a Nikon Ti2 fluorescence microscope with the excitation wavelength set from 380 nm to 417 nm, and two emission wavelengths set at 422 nm to 463 nm (blue) and from 654 nm to 734 nm (red), respectively. Each image was acquired with an exposure time of 200 ms and a 40X magnification. The fluorescence intensity of a cell was defined as Mean gray value = Integrated Density/Area and measured using Image J software (Figure 4c). We segmented the cells of interest manually and the area of the cell and the mean gray value were automatically calculated by Image J. Three different cells were collected for analysis at each AAs concentration to obtain an average and standard deviation.

ASSOCIATED CONTENT

Supporting Information Additional XRD result of Si/SiO₂ composite and FT-IR result of surface-oxide SiNCs; detailed ¹H NMR analysis of Schiff base reaction on SiNCs; additional HAADF-STEM images and analysis of SiNCs; the photographs indicate the color-switchable property and improved water solubility; Additional FT-IR and PL results based on Schiff base reaction of SiNCs, additional cell-incubation results.

AUTHOR INFORMATION

Corresponding Author

*Address correspondence to yangzhy63@mail.sysu.edu.cn.

Notes

Conflict of Interest: A provisional patent application CN110878203B was filed on June 15, 2021 by Sun Yat-sen University.

ACKNOWLEDGMENT

H.C. and J.X. contributed equally to this work. H.C., J.X., J.P., and Z.Y. designed and directed the study. H.C. led the synthesis and surface functionalization of SiNCs and the data analysis. J.X. and R.F-E. led the cell experiments, data collection, and interpretation. R.F-E., X.Y., and L.Z. designed and optimized the protocols for the cell experiments. D.W., A.P.T., and S.B. carried out TEM characterizations and data interpretation. H.C., Y.W., M.Y., and S.C. optimized the conditions of intercellular color-switching experiments. J.Z. and I.S. carried out the PLQY measurement, PL lifetime test, and data analysis. H.C., J.X., R.F-E, X.Y., J.P., and Z.Y. wrote the manuscript. All authors contributed to and commented on the paper. Z.Y. thank the financial support from the National Natural Science Foundation of China (Funding No.: 21905316), Guangdong Natural

Science Foundation (Funding No.: 2019A1515011748), the Science and Technology Planning Project of Guangdong Province (Funding No.: 2019A050510018), and Sun Yat-sen University.

REFERENCES

1. Kobayashi, H.; Choyke, PL. Target-Cancer-Cell-Specific Activatable Fluorescence Imaging Probes: Rational Design and In Vivo Applications. *Acc. Chem. Res.* **2011**, 44, 83-90.
2. Kamiya, M.; Urano, Y. Rapid and Sensitive Fluorescent Imaging of Tiny Tumors In Vivo and in Clinical Specimens. *Curr. Opin. Chem. Biol.* **2016**, 33, 9-15.
3. Daniel, G; Stefan, S.; Hans, G. L.; Niko, H. et al. Six-Colour Time-Resolved Förster Resonance Energy Transfer for Ultrasensitive Multiplexed Biosensing. *J. Am. Chem. Soc.* **2013**, 135, 1102-1109.
4. Kitoh-Nishioka, H.; Yokogawa, D.; Irle, S. Förster Resonance Energy Transfer Between Fluorescent Proteins: Efficient Transition Charge-Based Study. *J. Phys. Chem. A.* **2017**, 121, 4220-4238.
5. Stein, I. H.; Steinhauer, C.; Tinnefeld, P. Single-Molecule Four-Colour FRET Visualizes Energy-Transfer Paths on DNA Origami. *J. Am. Chem. Soc.* **2011**, 133, 4193-4195.
6. Jares-Erijman, E.; Jovin, T.M. FRET Imaging. *Nat. Biotechnol.* **2003**, 21, 1387-1395.
7. Liu, H.; Gu, Y.; Dai, Y.; Wang, K.; Zhang, S.; Chen, G.; Zou, B, Yang, B. Pressure-Induced Blue-Shifted and Enhanced Emission: A Cooperative Effect Between Aggregation-Induced Emission and Energy-Transfer Suppression. *J. Am. Chem. Soc.* **2020**, 142, 1153-1158.
8. Gao, M.; Su, H.; Lin, Y.; Ling, X.; Li, S.; Qin, A.; Tang, B. Photoactivatable Aggregation-Induced Emission Probes For Lipid Droplets-Specific Live Cell Imaging. *Chem. Sci.* **2017**, 8, 1763-1768.
9. Bruchez, M.; Moronne, M.; Gin, P.; Weiss, S.; Alivisatos, A. P. Semiconductor Nanocrystals as Fluorescent Biological Labels. *Science* **1998**, 281, 2013-2016.
10. Chan, W. C. W.; Nie, S. Quantum Dot Bioconjugates for Ultrasensitive Nonisotopic Detection. *Science* **1998**, 281, 2016-2018.

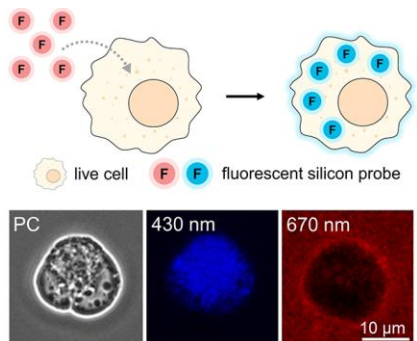
11. Medintz, I. L.; Uyeda, H. T.; Goldman, E. R.; Mattoussi, H. Quantum Dot Bioconjugates for Imaging, labelling and sensing. *Nat. Mater.* **2005**, 4, 435-446.
12. Dahan, M.; Sabine, L.; Camilla, L.; Philippe, R.; Béatrice, R.; Antoine, T. Diffusion Dynamics of Glycine Receptors Revealed by Single-Quantum Dot Tracking. *Science* **2003**, 302, 442-445.
13. Henderson, E. J.; Shuhendler, A. J.; Prasad, P.; Baumann, V.; Maier-Flaig, F.; Faulkner, D. O.; Lemmer, U.; Wu, X.; Ozin, G. A. Colloidally Stable Silicon Nanocrystals with Near-Infrared Photoluminescence for Biological Fluorescence Imaging. *Small* **2011**, 7, 2507-2516.
14. Gonzalez, C. M.; Veinot, J. G. C. Silicon Nanocrystals for the Development of Sensing Platforms. *J. Mater. Chem. C* **2016**, 4, 4836-4846.
15. Erogbogbo, F.; Yong, K.; Roy, I.; Xu, G.; Prasad, P. N.; Swihartaet, M. T. Biocompatible Luminescent Silicon Quantum Dots for Imaging of Cancer Cells. *ACS Nano* **2008**, 2, 873-878.
16. Dasog, M.; Kehrle, J.; Rieger, B.; Veinot, J. G. C. Silicon Nanocrystals and Silicon-Polymer Hybrids: Synthesis, Surface Engineering, and Applications. *Angew. Chem. Int. Ed.* **2016**, 55, 2322-2339.
17. Park J. H.; Gu, L.; Maltzahn, G. V. Ruoslahti, E.; Bhatia, S. N.; Sailor, M. J. Biodegradable Luminescent Porous Silicon Nanoparticles for In Vivo Applications. *Nat. Mater.* **2009**, 8, 331-336.
18. Cheng, X.; Lowe, S. B.; Reece, P. J.; Gooding, J. J. Colloidal Silicon Quantum Dots: From Preparation to the Modification of Self-Assembled Monolayers (SAMs) for Bio-Applications. *Chem. Soc. Rev.* **2014**, 43, 2680-2700.
19. Zhong, Y.; Peng, F.; Bao, F.; Wang, S.; Ji, X.; Yang, L.; Su, Y.; Lee, S. T.; He, Y. Large-Scale Aqueous Synthesis of Fluorescent and Biocompatible Silicon Nanoparticles and Their Use As Highly Photostable Biological Probes. *J. Am. Chem. Soc.* **2013**, 135, 8350-8356.

20. Dohnalová, K.; Poddubny, A. N.; Prokofiev, A. A.; Boer, W. D.; Umesh, C. P.; Paulusse, J. M.; Zuilhof, H.; Gregorkiewicz, T. Surface Brightens Up Si Quantum Dots: Direct Bandgap-Like Size-Tunable Emission. *Light Sci. Appl.* **2013**, *2*, e47-e47.
21. Dasog, M.; De los R. G.; Titova, L. V.; Hegmann, F. A.; Veinot, J. G. C. Size vs Surface: Tuning the Photoluminescence of Freestanding Silicon Nanocrystals Across the Visible Spectrum Via Surface Groups. *ACS Nano* **2014**, *8*, 9636-9648.
22. Dasog, M.; Yang, Z.; Regli, S.; Atkins, T. M.; Faramus, A.; Singh, M. P.; Muthuswamy, E.; Kauzlarich, S. M.; Tilley, R. D.; Veinot, J. G. C. Chemical Insight Into the Origin of Red and Blue Photoluminescence Arising From Freestanding Silicon Nanocrystals. *ACS Nano* **2013**, *7*, 2676-2685.
23. da Silva C. M.; da Silva, D. L.; Modolo, L. V.; Alvesa, R. B.; de Resende, M. A.; Martins, C. V. B.; de Fátimaet, A. Schiff bases: A Short Review of Their Antimicrobial Activities. *J. Adv. Res.* **2011**, *2*, 1-8.
24. Liu Q.; Yang, X.; Huang, Y.; Xu, S.; Su, X.; Pan, X.; Xu, J.; Wang, A.; Liang, C.; Wang, X.; Zhang, T. A Schiff Base Modified Gold Catalyst For Green and Efficient H₂ Production From Formic Acid. *Energy Environ. Sci.* **2015**, *8*, 3204-3207.
25. Piotr, P.; Adam, Huczynski.; Krystian, Pyta.; Bogumil, Brzezinski.; Franz, Bartlet. Biological Properties of Schiff Bases and Azo Derivatives of Phenols. *Curr. Org. Chem.* **2009**, *13*, 124-148.
26. Wei, L.; Tan, W.; Wang, G.; Li, Q.; Dong, F.; Guo, Z. The Antioxidant and Antifungal Activity of Chitosan Derivatives Bearing Schiff Bases and Quaternary Ammonium Salts. *Carbohydr. Polym.* **2019**, *226*, 115256.
27. Buriak, J. M. Organometallic Chemistry on Silicon and Germanium Surfaces. *Chem. Rev.* **2002**, *5*, 1271-1308.
28. Permatasari, F. A.; Aimon, A. H.; Iskandar, F.; Ogi, T.; Okuyama, K. Role of C–N Configurations in the Photoluminescence of Graphene Quantum Dots Synthesized by a Hydrothermal Route. *Sci. Rep.* **2016**, *6*, 21042.

29. Sychugov, I.; Pevero, F.; Luo, J.; Zunger, A.; Linnros, J. Single-Dot Absorption Spectroscopy and Theory of Silicon Nanocrystals. *Phys. Rev. B* **2016**, 93, 161413.
30. Tabbal, M.; Mérela, P.; Moisa, S.; Chaker, M.; Gat, E.; Ricard, A.; Moisan, M.; Gujrathic, S. XPS and FTIR Analysis of Nitrogen Incorporation in CN_x Thin Films. *Surf. Coat. Technol.* **1998**, 98, 1092-1096.
31. Bahrami, B.; Komvokis, V. G.; Singh, U. G.; Ziebarth, M. S.; Alexeev, O. S.; Amiridis, M. D. In Situ FTIR Characterization of NH₃ Adsorption and Reaction With O₂ and CO on Pd-Based FCC Emission Control Additives. *Appl. Catal., A* **2011**, 391, 11-21.
32. Liedberg, B.; Carlsson, C.; Lundström, I. An Infrared Reflection—Absorption Study of Amino Acids Adsorbed on Metal Surfaces: L-Histidine and L-Phenylalanine on Gold and Copper. *J. Colloid Interface Sci.* **1987**, 120, 64-75.
33. Dasog, M.; Veinot, J. G. C. Size Independent Blue Luminescence In Nitrogen Passivated Silicon Nanocrystals. *Phys. Status Solidi A*. **2012**, 209, 1844-1846.
34. Yang, Z.; De los Reyes, G.; Titova, L. V.; Sychugov, I.; Dasog, M.; Linnros, J.; Hegmann, F. A.; Veinot, J. G. C. Evolution of the Ultrafast Photoluminescence of Colloidal Silicon Nanocrystals With Changing Surface Chemistry. *ACS Photonics* **2015**, 2, 595-605.
35. Posakony, J. W.; England, J. M.; Attardi, G.; Mitochondrial Growth and Division During the Cell Cycle in HeLa Cells. *J. Cell Biol.* **1977**, 74, 468-491.
36. Todkar, K.; Ilamathi, H. S.; Germain, M. Mitochondria and Lysosomes: Discovering Bonds. *Front. Cell Dev. Biol.* **2017**, 5.
37. McCarthy, B. J.; Holland, J. J. Denatured DNA as a Direct Template for In Vitro Protein Synthesis. *Proc. Natl. Acad. Sci. U.S.A.* **1965**, 54, 880-886.
38. Garrabou, X.; Wicky, B. I. M.; Hilvert, D. Fast Knoevenagel Condensations Catalyzed by an Artificial Schiff-Base-Forming Enzyme. *J. Am. Chem. Soc.* **2016**, 138, 6972-6974.
39. Ueno, T.; Nagano, T. Fluorescent Probes for Sensing and Imaging. *Nat. Methods* **2011**, 8, 642-645.

40. Zhu, H.; Fan, J.; Du, J.; Peng, X. Fluorescent Probes for Sensing and Imaging within Specific Cellular Organelles. *Acc. Chem. Res.* **2016**, 49, 2115-2126.
41. Clark, R. J.; Aghajamali, M.; Gonzalez, C. M.; Hadidi, L.; Islam, M. A.; Javadi, M.; Mobarok, M. H.; Purkait, T. K.; Robidillo, C. J. T.; Sinelnikov, R.; Thiessen, A. N.; Washington, J.; Yu, H.; Veinot, J. G. C. From hydrogen silsesquioxane to functionalized silicon nanocrystals. *Chem. Mater.* **2016**, 29, 80-89.

Table of Contents



Supporting Information

Color-Switchable Nano-Silicon Fluorescent Probes

Huai Chen^{§1}, † Jiang Xu^{§2}, Yaping Wang¹, Da Wang³, Raquel Ferrer-Espada², Yutong Wang⁴, Jingjian Zhou⁵, Adrián Pedraza-Tardajos³, Mei Yang⁴, Jia-Heng Tan⁶, Xiaoyu Yang⁷, Lei Zhang⁸, Ilya Sychugov⁵, Shoudeng Chen⁴, Sara Bals³, Johan Paulsson², Zhenyu Yang^{*1}

1. MOE Laboratory of Bioinorganic and Synthetic Chemistry, Lehn Institute of Functional Materials, School of Chemistry, Sun Yat-sen University, Guangzhou, 510275, China
2. Department of Systems Biology, Blavatnik Institute, Harvard Medical School, Boston, MA, 02115, USA
3. EMAT and NANOlaboratory Center of Excellence, University of Antwerp, B-2020 Antwerp, Belgium, Groenenborgerlaan 171, 2020 Antwerp, Belgium
4. Guangdong Provincial Key Laboratory of Biomedical Imaging, the Fifth Affiliated Hospital, Sun Yat-sen University, Zhuhai, 519000, China
5. Department of Applied Physics, KTH Royal Institute of Technology, 11419 Stockholm, Sweden
6. School of Pharmaceutical Sciences, Sun Yat-sen University, Guangzhou, 510275, China
7. Department of Molecular Medicine, School of Medicine, University of Texas Health Science Center at San Antonio, San Antonio, TX, 78229, USA
8. Department of Chemical Engineering, Waterloo Institute for Nanotechnology, University of Waterloo, 200 University Avenue West, Waterloo, ON N2L3G1, Canada

§ Indicates equal contribution

Corresponding E-mail: yangzhy63@mail.sysu.edu.cn

Table S1. Summary of photoluminescence quantum yield (PLQY) and PL lifetime values of functionalized SiNC solutions. Note that the value of Beta (β) reflected the stretched exponential function by inserting a fractional power law into the exponential function. Note*: The stretched exponential function could be described as $f_{\beta}(t) = e^{-(t/t_0)^{\beta}}$. The closer β is to 1, the narrower the lifetime distribution in SiNCs is.

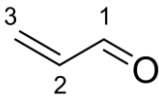
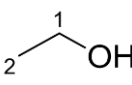
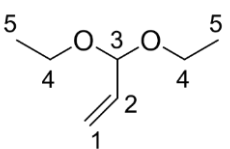
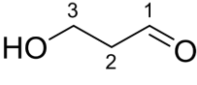
Sample	Solvent	λ_{ex}	$\lambda_{em\ max}$	PLQY (%)	PL lifetime, t_0	Beta*
A-SiNCs	chloroform	380 nm	850 nm	25	70 μ s	1.00
Gly-A-SiNCs	H ₂ O	380 nm	440 nm	≤ 5	5 ns	0.73
Thr-A-SiNCs	H ₂ O	380 nm	450 nm	≤ 5	3 ns	0.61
Cys-A-SiNCs	H ₂ O	380 nm	460 nm	≤ 5	4 ns	0.89
His-A-SiNCs	H ₂ O	380 nm	465 nm	≤ 5	3 ns	0.62
GFR-A-SiNCs	H ₂ O	380 nm	470 nm	-	7 ns	-
BA-SiNCs	toluene	380 nm	465 nm	≤ 5	5 ns	0.77

Table S2. Formulation of the cell culture media.

Aminoacids	50x ($\mu\text{g/mL}$)	1x ($\mu\text{g/mL}$)	0.75x ($\mu\text{g/mL}$)	0.5x ($\mu\text{g/mL}$)	0.25x ($\mu\text{g/mL}$)
L-Arginine (free base)	10000	200	150	100	50
L-Asparagine•H ₂ O	2840.65	56.813	42.60975	28.4065	14.20325
L-Aspartic Acid	1000	20	15	10	5
L-Cystine	2500	50	37.5	25	12.5
L-Glutamic Acid	1000	20	15	10	5
Glycine	500	10	7.5	5	2.5
L-Histidine (free base)	750	15	11.25	7.5	3.75
Hydroxy-L-Proline	1000	20	15	10	5
L-Isoleucine	2500	50	37.5	25	12.5
L-Leucine	2500	50	37.5	25	12.5
L-Lysine•HCl	2000	40	30	20	10
L-Methionine	750	15	11.25	7.5	3.75
L-Phenilalanine	750	15	11.25	7.5	3.75
L-Proline	1000	20	15	10	5
L-Serine	1500	30	22.5	15	7.5
L-Threonine	1000	20	15	10	5
L-Tryptophan	250	5	37.5	2.5	1.25
L-Tyrosine	1159.86	23.1972	17.3979	11.5986	5.7993
L-Valine	1000	20	15	10	5
L-Glutamine	-	300	225	150	75
Total Aminoacids	-	994	745.5	497	248.5
Vitamins					
Biotin	-	0.2	-	-	-
Choline chloride	-	3	-	-	-
D-Calcium pantothenate	-	0.25	-	-	-
Folic Acid	-	1	-	-	-
Niacinamide	-	1	-	-	-
Para-Aminobenzoic Acid	-	1	-	-	-
Pyridoxine hydrochloride	-	1	-	-	-
Riboflavin	-	0.2	-	-	-
Thiamine hydrochloride	-	1	-	-	-
Vitamin B12	-	0.005	-	-	-
i-Inositol	-	35	-	-	-
Inorganic Salts					
Calcium nitrate (Ca(NO ₃) ₂ •4H ₂ O)	-	100	-	-	-
Magnesium Sulfate (MgSO ₄) (anhyd.)	-	48.84	-	-	-
Potassium Chloride (KCl)	-	400	-	-	-
Sodium Bicarbonate	-	2000	-	-	-

(NaHCO ₃)					
Sodium Chloride (NaCl)	-	5300	-	-	-
Sodium Phosphate dibasic (Na ₂ HPO ₄) anhydrous	-	800	-	-	-
Other Components					
D-Glucose (Dextrose)	-	2000	-	-	-
Glutathione (reduced)	-	1	-	-	-
HEPES	-	5958	-	-	-
Phenol Red	-	5	-	-	-

Table S3. ¹H NMR characteristics of compounds in hydrolysis of 3,3-diethoxy propene.

Compound	Signal	Chemical shift (ppm)	Multiplicity	Spectral prediction	Relative intensity
 acrolein	H-C (1) H-C (2) H-C (3) cis H-C (3) trans	9.51 6.20-6.40 6.46 6.44	d m d d	9.68 6.21 6.27 6.27	1 1 1 1
 ethanol	H-C (1) H-C (2)	3.63 1.17	m t	3.65 1.10	2 3
 3,3-diethoxy propene	H-C (1) cis H-C (1) trans H-C (2) H-C (3) H-C (4) H-C (5)	5.30 5.20 5.85 4.80 3.50 1.10	t t m t m t	5.41 5.16 5.89 4.88 3.50 1.10	1 1 2 1 2 3
 3-hydroxypropionaldehyde	H-C (1) H-C (2) H-C (3)	9.79 2.61 3.71	t t t	9.72 2.59 3.86	1 2 2

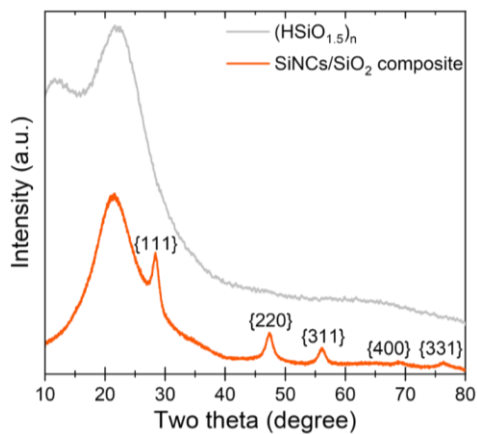


Figure S1. XRD patterns of $(\text{HSiO}_{1.5})_n$ precursor and SiNCs/SiO₂ composite processed at 1100°C for 1 h. Broad signals at $2\theta = 22^\circ$ may originate from the amorphous silicon oxide matrix.

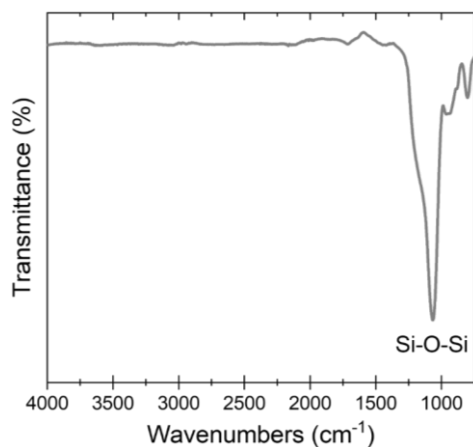


Figure S2. FT-IR spectrum of SiNCs after control radical initiation reaction. The reaction between hydride-terminated SiNCs and the radical initiator AVDN (i.e., without the presence of functional ligand acrolein) only yields surface-oxidized SiNCs.

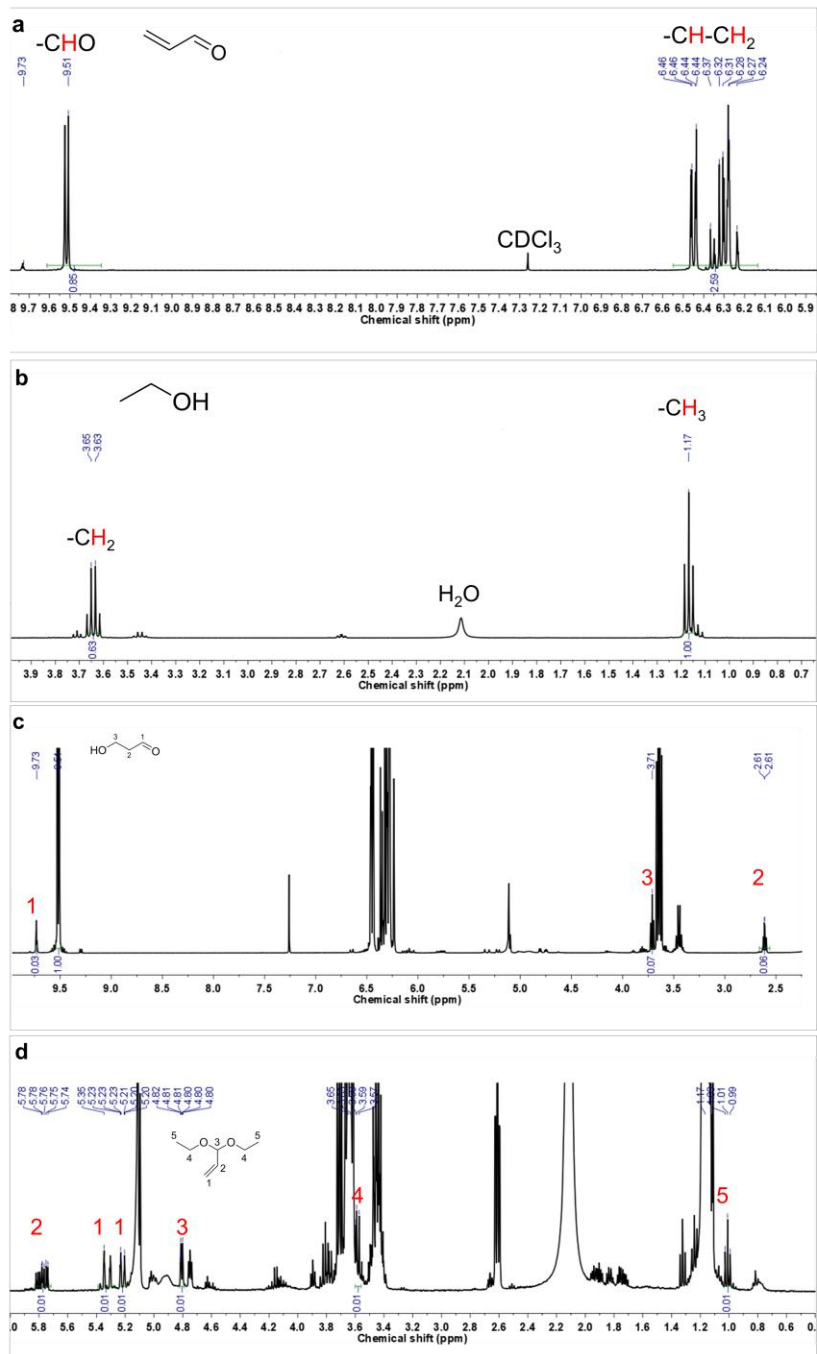


Figure S3. Liquid-state $^1\text{H-NMR}$ analysis of as-prepared acrolein. Zoom-in area of $^1\text{H-NMR}$ spectra of (a) acrolein, (b) ethanol, (c) 3-hydroxypropionaldehyde and (d) 3,3-diethoxy propene dispersed in CDCl_3 .

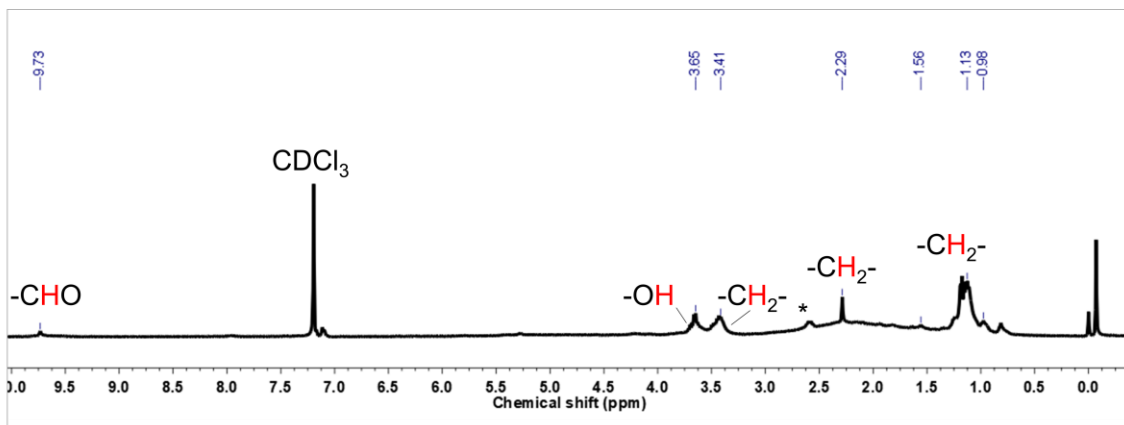


Figure S4. $^1\text{H-NMR}$ spectra of A-SiNCs dispersed in CDCl_3 . Chemical shifts at 9-10 ppm are assigned to the aldehyde group.

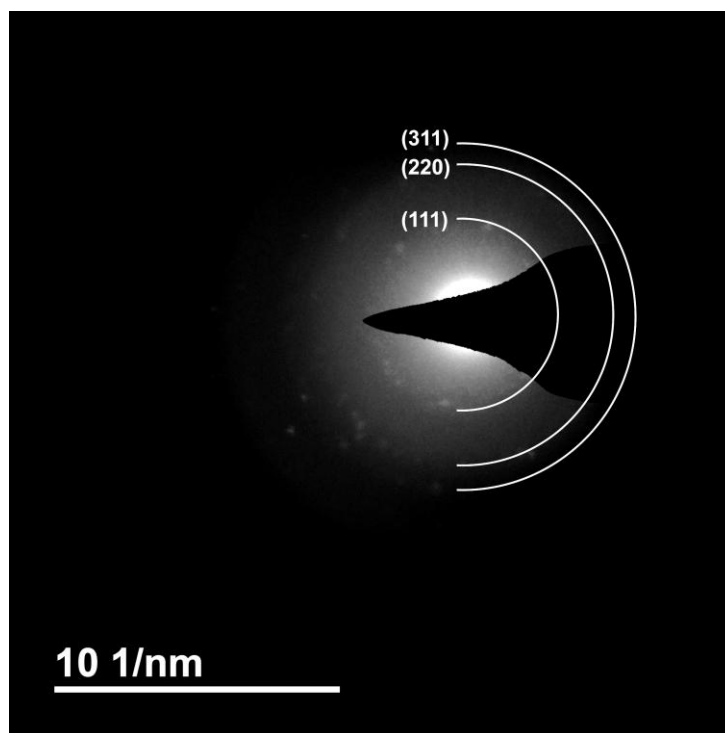


Figure S5. Selected area electron diffraction (SAED). A SAED image of A-SiNCs, showing the (111), (220) and (311) reflections of Si.

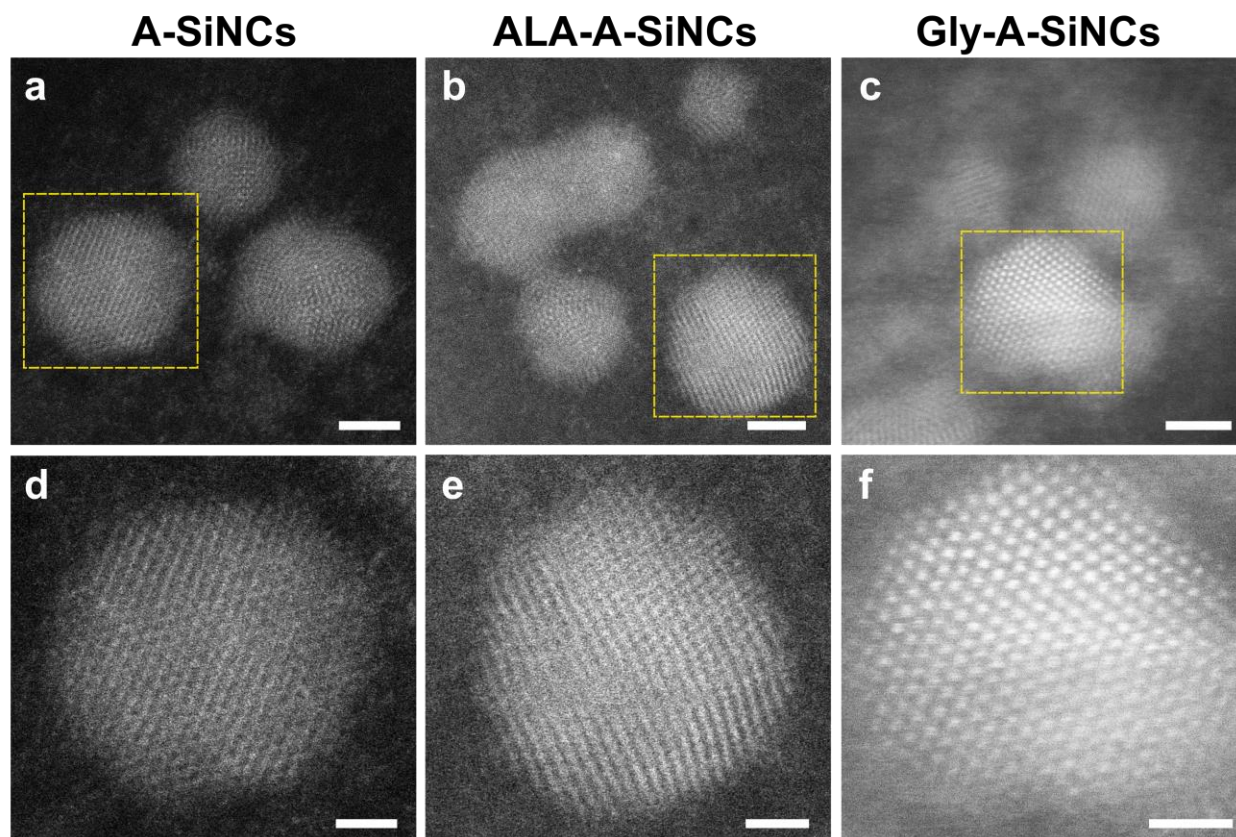


Figure S6. High-resolution STEM images of SiNCs. HAADF-STEM images of (a,d) A-SiNCs, (b,e) ALA-A-SiNCs, and (c,f) Gly-A-SiNCs. Scale bars, a-c) 2 nm and d-f) 1 nm.

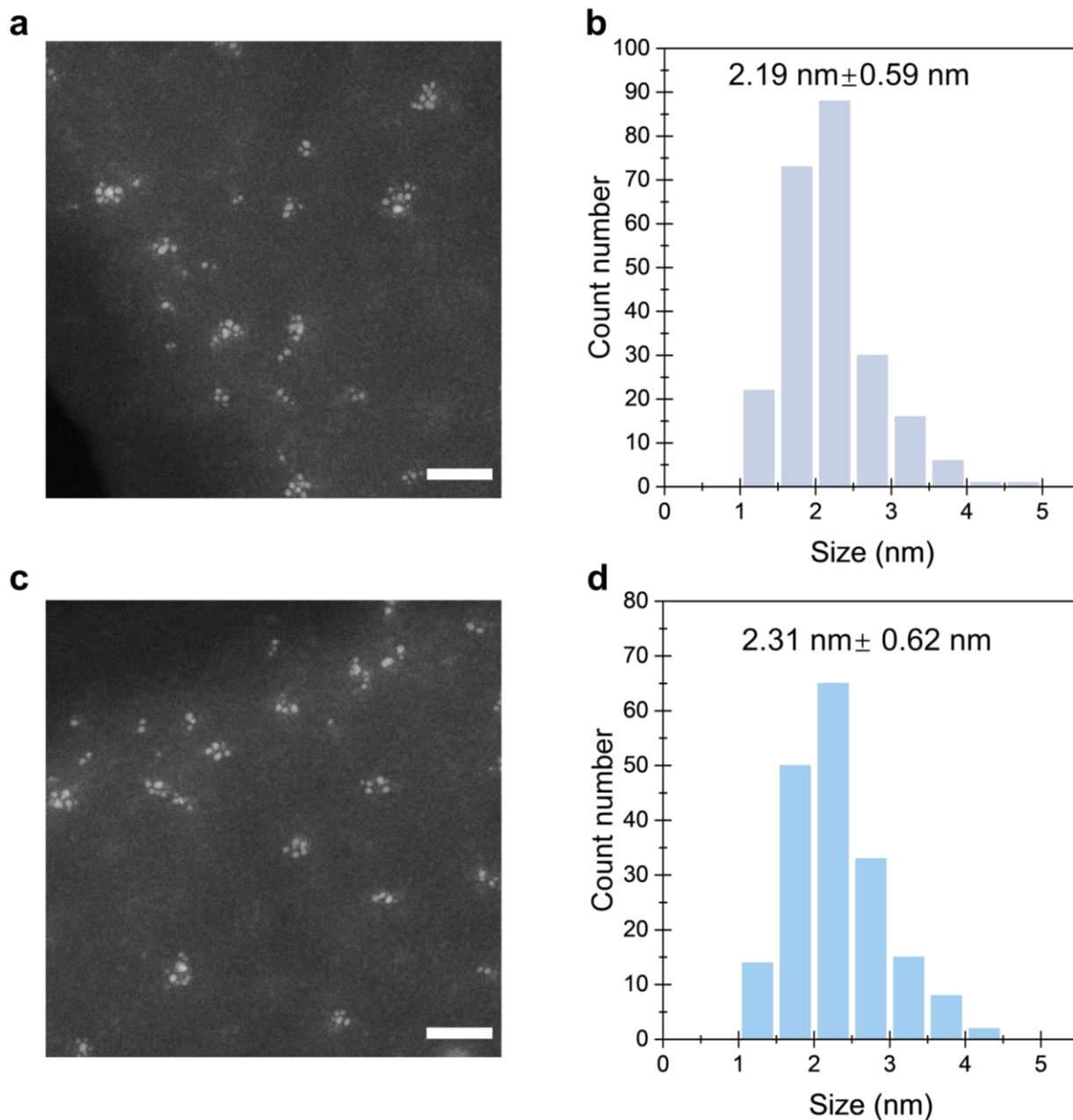


Figure S7. HAADF-STEM images and the corresponding particle size distribution of (a-b) A-SiNCs (number of measured particles: 235), and (c-d) ALA-A-SiNCs (number of measured particles: 187). The average sizes and their corresponding standard deviations were calculated based on the measurement from more than 180 particles by the software Fiji. Scale bar = 20 nm.

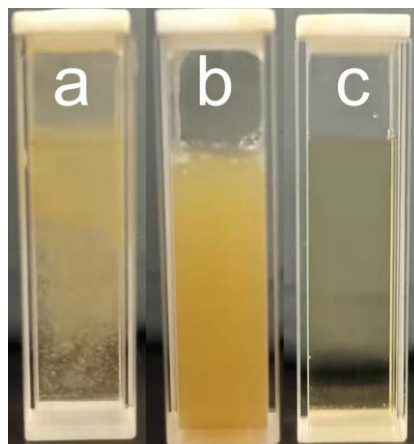


Figure S8. The dispersity of various types of SiNCs in water. (a) hydride-terminated SiNCs, (b) A-SiNCs, and (c) Gly-A-SiNCs.

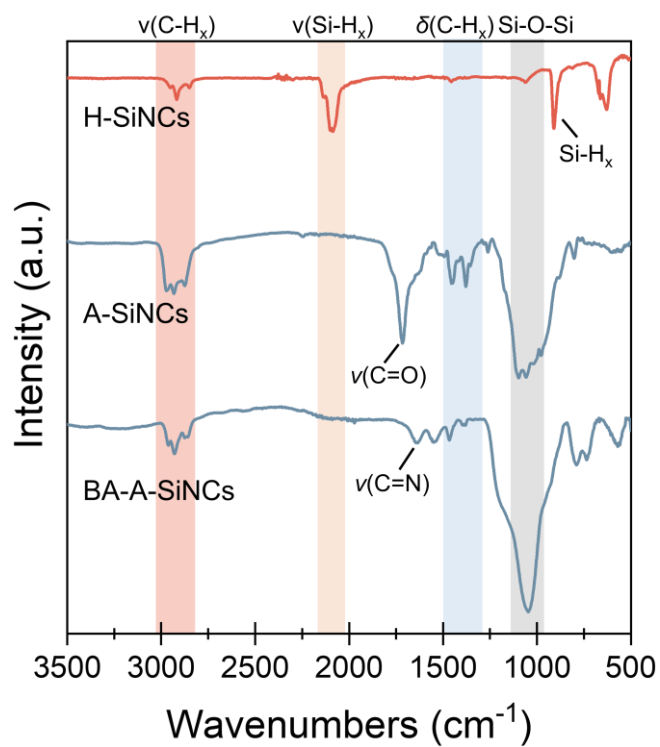


Figure S9. FT-IR spectra of H-SiNCs, A-SiNCs, and BA-A-SiNCs.

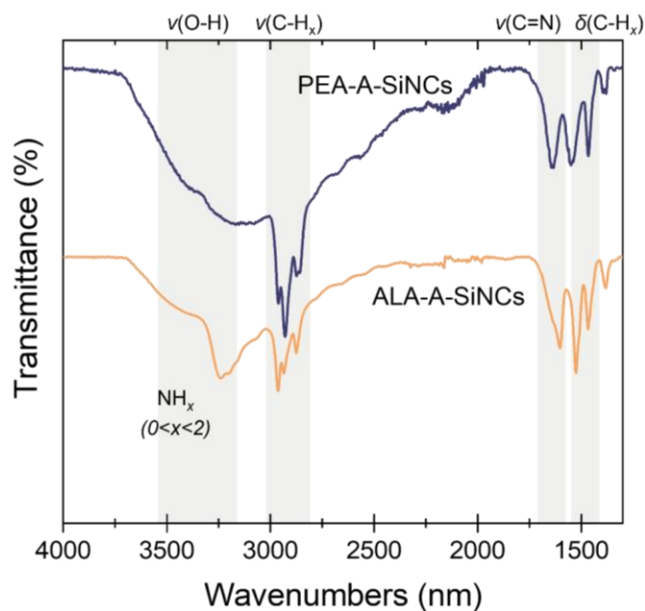


Figure S10. FT-IR spectra of allylamine and phenylethylamine functionalized SiNCs.

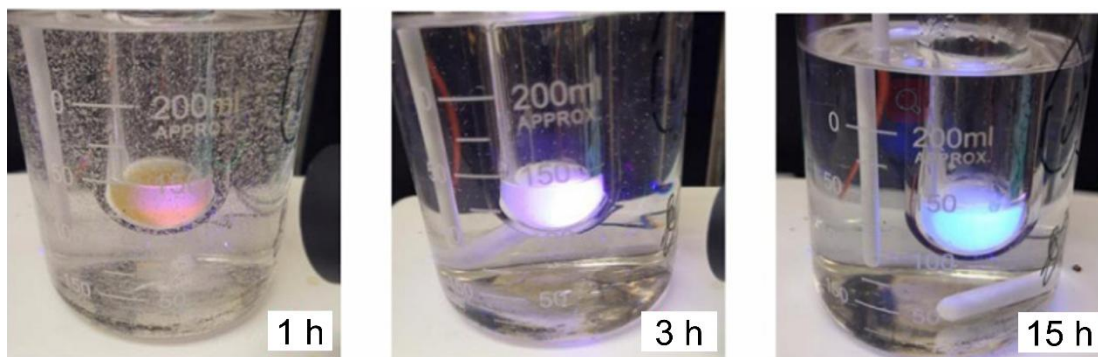


Figure S11. Pictures of A-SiNCs solution under the Schiff base reaction with glycine at 77°C with various processing times. The change of the PL color is evident when irradiated using 365 nm UV light.

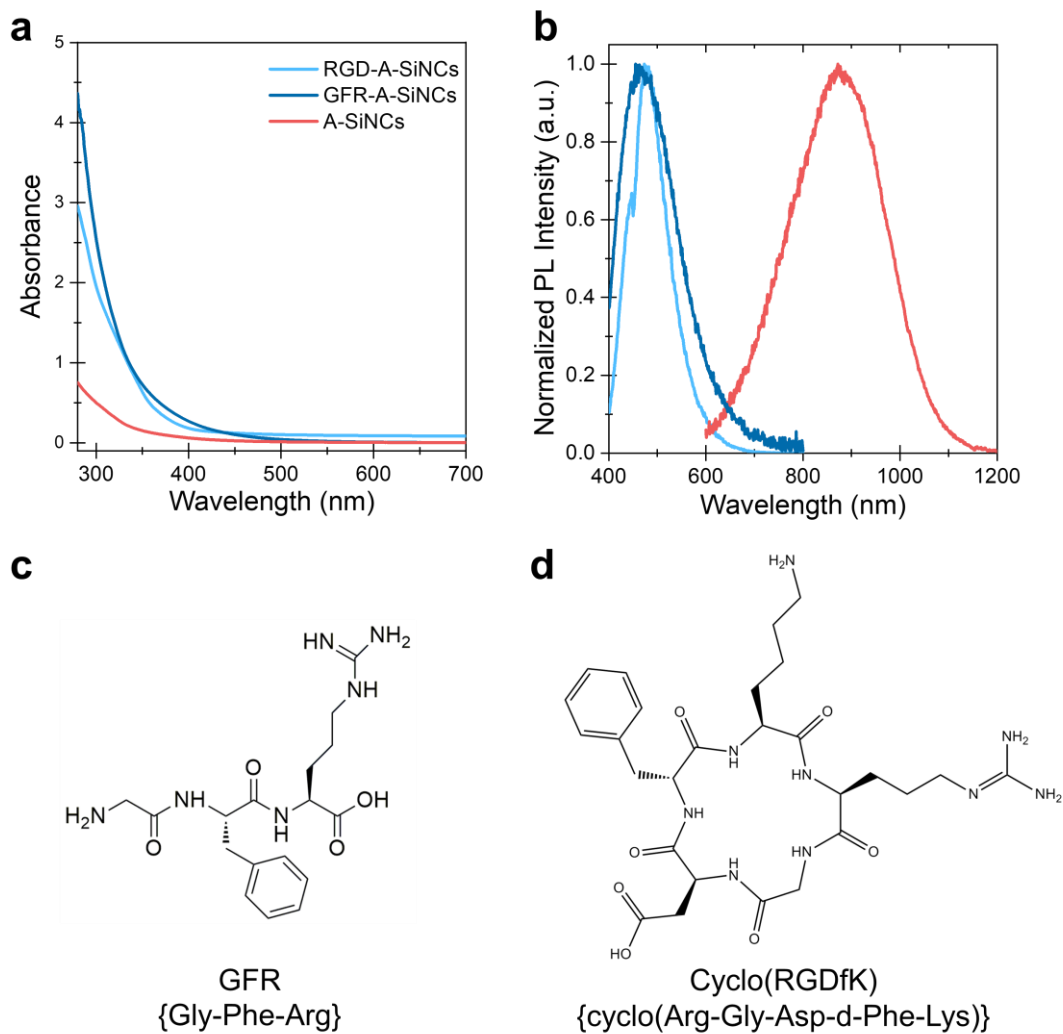


Figure S12. Photophysical properties of peptide-anchored SiNCs. (a) Absorption and (b) PL spectra of SiNCs before and after the Schiff base reaction with GFR and RGD peptides. (c) and (d) are molecular structures of GFR peptide (peptide sequence: Gly-Phe-Arg) and RGD peptide (peptide sequence: cyclo RGDfK (Arg-Gly-Asp-d-Phe-Lys)).

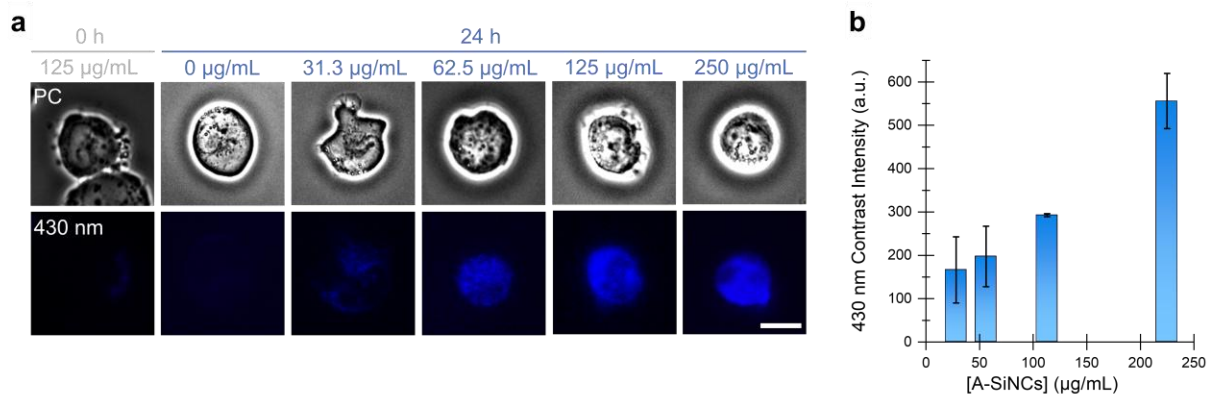


Figure S13. Color-switchable probing with various concentrations of A-SiNCs. (a) Fluorescence microscopy images of OCI-AML-2 cells before (0 h) and after incubation (24 h) with various concentrations of A-SiNCs (0, 31.25, 62.5, 125 and 250 µg/mL). The concentration of AAs is 994 µg/mL. The PL signal was detected at 430 nm (blue) and excitation wavelength range between 387 and 417 nm, scale bar: 10 µm). (b) BR PL intensity collected from cell samples listed in Figure S12a. The contrast intensity equals to the measured intensity minus that of the control group (i.e., 0 µg/mL, 24 h incubation). Each measurement was repeated three times to obtain an average and standard deviation.

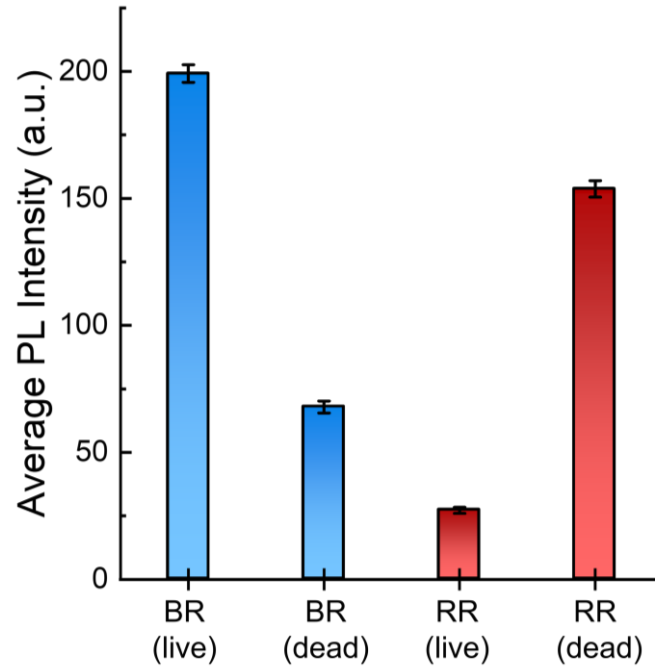


Figure S14. The corresponding average signal intensity of both blue and red channels in living and dead cells in the fluorescence images with the presence of A-SiNCs shown in Figure 5d.